Journal of Sound and Vibration 413 (2018) 79–100

Contents lists available at ScienceDirect

Journal of Sound and Vibration

journal homepage: www.elsevier.com/locate/jsvi

On the non-proportionality between wheel/rail contact forces and speed during wheelset passage over specific welds

Nekane Correa, Ernesto G. Vadillo*, Javier Santamaria, Julio Blanco-Lorenzo

Department of Mechanical Engineering, University of the Basque Country UPV/EHU, Escuela Técnica Superior de Ingeniería, Alda Urquijo s/n, 48013 Bilbao, Spain

ARTICLE INFO

Article history:
Received 22 November 2016
Received in revised form 17 October 2017
Accepted 19 October 2017
Available online 16 November 2017

Keywords:
Wheel-rail contact
Rail defects
Welds
Wheel-rail forces

ABSTRACT

This study investigates the influence on the wheel-rail contact forces of the running speed and the shape and position of weld defects along the track. For this purpose, a vertical dynamic model in the space domain is used. The model is obtained from the transformation between the domains of frequency and space using a Rational Fraction Polynomials (RFP) method, which is modified with multiobjective genetic algorithms in order to improve the fitting of track receptance and to assist integration during simulations. This produces a precise model with short calculation times, which is essential to this study. The wheel-rail contact is modelled using a non-linear Hertz spring. The contact forces are studied for several types of characteristic welds. The way in which forces vary as a function of weld position and running speed is studied for each type of weld. This paper studies some of the factors that affect the maximum forces when the vehicle moves over a rail weld, such as weld geometry, parametric excitation and contact stiffness. It is found that the maximum force in the wheel-rail contact when the vehicle moves over a weld is not always proportional to the running speed. The paper explains why it is not proportional in specific welds.

© 2017 The Authors. Published by Elsevier Ltd. This is an open access article under the CC BY-NC-ND license (http://creativecommons.org/licenses/by-nc-nd/4.0/).

1. Introduction

In recent years, studies have been conducted on the dynamic interaction between the rail vehicle and the track, when the former moves over irregularities on the latter, such as rail welds [1–5], corrugation [6–10], rail joints [11–13], general defects [14] and other general or special geometric flaws on the tracks [15,16]. Specifically, the presence of welds (Fig. 1) on track rails causes irregularities on the surface of the rail, which significantly affect the dynamic interaction between the rail vehicle and the track. These irregularities lead to fluctuations in the wheel-rail contact forces as the vehicle moves over the rail, and this can lead to detachment and impacts. This can induce rolling contact fatigue, causing cracks to initiate in the weld defects [17]. Defects on the rail can also be instrumental in the development of corrugations [18]. In fact, the presence of weld defects is a common trigger for rail corrugation [19]. All this makes it necessary to study the wheel-rail interaction that occurs when a vehicle moves over this type of defect on a rail surface.

* Corresponding author.
E-mail address: ernesto.garciavadillo@ehu.es (E.G. Vadillo).

https://doi.org/10.1016/j.jsv.2017.10.031
0022-460X/© 2017 The Authors. Published by Elsevier Ltd. This is an open access article under the CC BY-NC-ND license (http://creativecommons.org/licenses/by-nc-nd/4.0/).

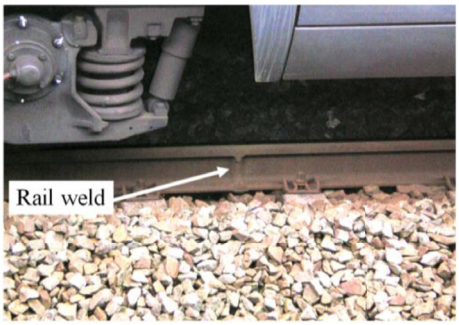

Fig. 1. Rail weld on a ballast track in Bilbao.

A time-domain model, which is capable of considering the nonlinearities in the wheel-rail contact force as the vehicle moves over the weld on a track with discrete supports, is required to carry out this study. In addition, the calculations have to be extremely rapid because the number of cases to be examined is considerably high (over 5000).

This study employs a time-domain model obtained by applying the Rational Fraction Polynomials (RFP) method [20]. This method enables a time-domain model to be developed from track information, which is in the frequency domain, such as track receptances. The RFP method can be used to fit the transfer functions in such a way that their associated receptances match the actual track receptances of different sections along the span. This setup is based on the Wu/Thompson model [21,22], which is modified to provide greater accuracy in the fittings of receptances at low frequencies. The low frequency range is precisely where the sleeper passing frequency is located, and this frequency is most important to the study carried out in this paper. The improvement is made using optimisation methods with multiobjective genetic algorithms. This produces a rapid and accurate wheel-track model, which has been validated and described in detail in Ref. [23]. The integration time of a wheelset passing over the weld is roughly 1 s. This enables an extremely rapid analysis of the contact forces between the wheelset and the rail. This model will be described in more detail in Section 2.1.

The consequences of the presence of welds on rail surfaces have been studied previously by other authors.

Steenbergen and Esveld [1] performed a study aimed at obtaining a new weld acceptance regulation. They proposed analytic expressions to calculate the contact forces when passing over rail welds. The assessment criterion for weld acceptance was based on the calculation of a quality index (QI) to determine whether the post-grinding weld geometry was acceptable. In order to assess the maximum contact forces, this criterion considers the first or second derivative of the geometry of the defect. This has proved to be more accurate in determining the validity of a weld than employing the criterion that the amplitudes of the defect should not exceed a certain value, which is the usual procedure in weld acceptance regulations. In Ref. [2] Steenbergen calculated the forces by an analytical expression, representing the welds as a sequence of discrete slopes. He also calculated the values of the P1 and P2 forces applied to rail welds.

In Ref. [5], Grossoni continues on the line of work of Steenbergen and Esveld through a series of parametric studies, and she also proposes to use a standard based on first-derivative based methods instead of the current zeroderivative methods.

In Ref. [4], Wen et al. showed the values of contact forces produced by wheelset passage over idealised rail welds, at high speeds only. They found that the trend of the maximum forces during wheelset passage over welds was practically linear, and that they increased as speed increased. These researchers, however, only analysed one type of defect (the one having the shape of a cosine function). This means that the welds are idealised, and although the authors of [4] modified the wavelengths and amplitudes of the cosines, they did not present any results for real welds, the shapes of which are more complicated.

This study analyses wheel-rail contact forces during wheelset passage over welds. It may initially be thought that, as the ride speed over a weld defect increases, the maximum wheel-rail contact forces would increase linearly. This does occur with some rail defects, such as rail dipped joints [11,13,24], where both P1 and P2 show a linear increase with speed. However, this is not always the case with rail welds. In some situations, the maximum contact forces during wheelset passage over welds do not increase linearly; instead, the maximum force may remain constant or even diminish as the running speed increases, as it was shown in Ref. [25]. It was found that the maximum contact forces increased up to a certain speed, at which the curve reached a maximum. Subsequently, it decreased and then increased again.

Similar results were obtained in Refs. [26–30] for the scenario of a wheel flat defect in the interaction between the wheel and rail. Fig. 2 shows the results of the maximum contact force obtained from the experiments [28] for a wheel flat. It can be observed that, at low speeds, the maximum contact force increases as running speed increases. However, above speeds of approximately 40 km/h, a higher ride speed does not produce a higher maximum contact force, which in fact falls to a relative minimum at around 95 km/h. After the relative minimum, it appears that the maximum force/speed curve recovers its initial upward trend.

In this study, an in-depth analysis is conducted on the different types of the most representative welds that have been used throughout the paper. Some of them have been measured in the vicinity of Bilbao – all of which are aluminothermic welds – and the others have been taken from the studies mentioned in the bibliography. If the bibliographic source has specified

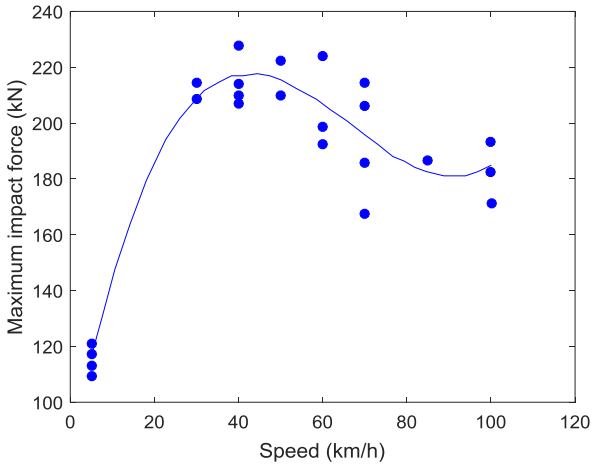

Fig. 2. Contact forces caused by a wheel flat measured experimentally by Johansson and Nielsen [28].

whether it is an aluminothermic or flash butt weld, this information has been added to this paper. It has been checked that none of the welding irregularities used throughout this paper implies double-point contact. For all the welds, it is ascertained whether or not they retain the shape of the maximum contact force curve with respect to the speed, as described above; that is, whether it rises to a relative maximum, decreases, and then rises again. An analysis is performed to determine whether the relative maximum value on this curve is present in all cases, or whether it is exclusive to certain types of welds. In addition, an investigation is performed to ascertain why the contact force becomes smaller as the speed increases for certain welds at a particular speed range. All these studies are carried out in consideration of the different positions at which welds may be located on the track span, in order to examine the differences on the curves.

Field-made welds are always made in the sleeper bay in order to insert the mould required for welding. However, in some new lines rails are received in situ with a maximum length of 12 or 18 m. Rails are provisionally mounted on the edge of the sleeper and aluminothermically welded to form the continuously welded rail (CWR). Once the CWR is created, the entire rail is placed in its final position (the grooves on the sleeper) and then fastened to the sleeper. Occasionally, some of the welds may be located over a sleeper. This can be seen in Fig. 3, taken from one of the railway lines in the vicinity of the University in Bilbao.

More than 5000 cases have been studied. The study also analyses how the wheel-rail forces are affected by various factors, such as the geometry of the weld and its decomposition in wavelengths, track parametric excitation due to its discrete support, dynamics of the wheelset-track system, and stiffness of the wheel-rail contact. The conclusions show the tendencies in the forces for each type of weld, and explain the reason for the frequent lack of proportionality between speed and maximum wheel-rail contact force.

The objective of this work is not to obtain a general formula for calculating the maximum contact forces during the passage over any weld. Instead, it aims to explain why in some cases a non-linear relation can be observed in the contact forces during the passage over welds, and the cases in which this occurs (those cases in which the welding geometry is characterised by a dip); and, on the contrary, in which cases the relationship between the maximum force and speed is linear, and the reason for this linearity. The criterion for choosing the geometry of welds shown in this paper has been to select from among all those analysed, some welds that give rise to a linear response of forces with respect to velocity and others that give rise to a nonlinear response.

2. Wheel-rail interaction model

To study the influence of weld defects and running speed on the contact forces, a wheel-rail interaction model was used, which is described in depth in Ref. [23]. This section provides a summary of this model, which is based on the RFP method. The RFP method applied to tracks was initially used by Wu and Thompson for tracks with continuous support [27,31] and for tracks with discrete support [21,22]. It was optimised in Ref. [23], greatly increasing the accuracy of receptance fitting, especially at low frequencies.

2.1. Track model

Track dynamics are modelled using a system of differential equations with variable coefficients. Specifically, these equations describe the dynamic behaviour of the point on the rail making contact with the wheel. This system of ordinary differential equations was obtained from the track receptances at different sections of the track between two sleepers. It is necessary to have information about the frequency response of the track at different sections, because the receptance at the

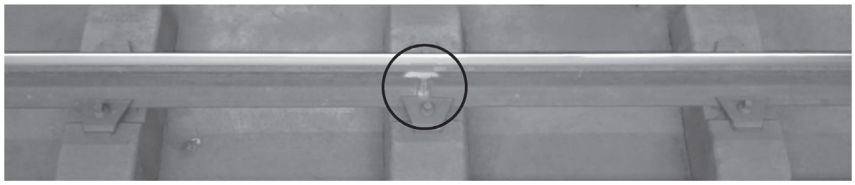

Fig. 3. Aluminothermic weld over the sleeper.

contact point changes as the contact point itself moves along the rail during the trajectory of the wheelset. These receptances are computed using a very precise and fast track model in the frequency domain, which is implemented in the RACING tool [32], based on the Periodic Structure Theory and the Finite Strip Method. During a second stage, a set of transfer functions (G) are fitted so that they have the same frequency response as that of the track receptances ($\mathbf{h}$). This is done using the RFP method [20]. In fact, this RFP method obtains the coefficients of a transfer function which fits the input data receptance. The transfer functions relate the Laplace transforms of the displacements on the upper point of the rail ($Z_r(S)$) and of the contact force ($F_c(S)$) between the wheel and rail (Eq. (1)).

$$G(S) = \frac{Z_r(S)}{F_c(S)} = \frac{b_1 S^7 + b_2 S^6 + \ldots + b_7 S + b_8}{S^8 + a_1 S^7 + \ldots + a_7 S + a_8} \tag{1}$$

These transfer functions, the number of which matches the track span sections on which the receptances were calculated, take the form of a polynomial quotient on the S plane (Laplace). In this case, it was sufficient to use polynomials of degrees 7 and 8. In some cases, it is necessary to use polynomials with higher degrees, depending on the number of resonances and anti-resonances in the track receptance within the frequency interval in which their fitting is being applied. For some track scenarios, numerator and denominator with degrees of less than 7 and 8, respectively, will suffice. Specifically, for tracks with continuous support, coefficients with degrees of up to 5 and 6 will suffice. The problem requires optimisation in order to fit the coefficients of the numerator and denominator polynomials of the transfer functions so that their associated receptances match the track receptances as closely as possible. The minimisation problem posed is shown in Eq. (2).

$$\min_{a,b} \sum_{k=1}^{p} \mathbf{wt}(k) \left| \mathbf{h}(\boldsymbol{\omega}(k)) - \frac{b_1 (j\boldsymbol{\omega}(k))^7 + b_2 (j\boldsymbol{\omega}(k))^6 + \ldots + b_6 (j\boldsymbol{\omega}(k))^2 + b_7 (j\boldsymbol{\omega}(k)) + b_8}{(j\boldsymbol{\omega}(k))^8 + a_1 (j\boldsymbol{\omega}(k))^7 + a_2 (j\boldsymbol{\omega}(k))^6 + \ldots + a_6 (j\boldsymbol{\omega}(k))^2 + a_7 (j\boldsymbol{\omega}(k)) + a_8} \right|^2 \tag{2}$$

As may be observed, this contains the **wt** variable, or weighting vector. In the process of fitting these receptances, the error at each frequency ($\boldsymbol{\omega}(k)$) is weighted using a weighting vector to achieve better results in the receptances and to obtain a system of differential equations that can be easily integrated. In the method developed in Ref. [23], this weighting vector is optimised using multiobjective genetic algorithms with two target functions: one to obtain a weighting vector for minimising the fitting error, and another to ensure that the coefficients of the fitted transfer functions are bounded.

Once the transfer functions have been fitted at the different positions along the track span, each transfer function may be transformed into an ordinary differential equation, as shown in Eq. (3a), where $z_r(t)$ and $f_c(t)$ are the vertical displacement of the rail and the wheel-rail contact force, respectively. This equation is obtained by applying the inverse Laplace transform to Eq. (1). In this case, the order of the differential equations arrived at is 8, the same as the degree of the polynomial in the denominator of the transfer function. This equation may in turn be replaced by a system of first order differential equations (Eq. (3b)). Although the appearance of these equations may be the same for all the positions on the span, the coefficients of the transfer functions change. Thus, a system of 8 first order ordinary differential equations with variable coefficients is obtained.

$$z_r^{8)}(t) + a_1 z_r^{7)}(t) + a_2 z_r^{6)}(t) + \ldots + a_7 z_r'(t) + a_8 z_r(t) = b_1 f_c^{7)}(t) + b_2 f_c^{6)}(t) + \ldots + b_6 f_c'(t) + b_7 f_c(t) \tag{3a}$$

$$\begin{aligned} z_1'(t) &= z_2(t) + c_1 f_c(t) \\ z_2'(t) &= z_3(t) + c_2 f_c(t) \\ &\ldots \\ z_7'(t) &= z_8(t) + c_7 f_c(t) \\ z_8'(t) &= -a_8 z_1(t) - a_7 z_2(t) - a_6 z_3(t) - \ldots - a_1 z_8(t) + c_8 f_c(t) \end{aligned} \tag{3b}$$

where the values corresponding to c and z_1 are:

$$\begin{aligned} c_1 &= b_1 \\ c_2 &= b_2 - a_1 c_1 \\ &\cdots \\ c_8 &= b_8 - \sum_{k=1}^{7} a_{8-k} c_k \\ z_r(t) &= z_1(t) \end{aligned} \tag{3c}$$

This model was validated by means of the experimental results of Johansson and Nielsen [28] and with Pieringer's numerical results [29,30], as shown in a following section. Pieringer's results are based on a model that uses Green's functions as in Refs. [33,34].

The parameters of the ballasted track used throughout the paper, except in the validation, are as follows [23]: pad stiffness 348.6 kN/mm, pad damping (loss factor) 0.29, ballast stiffness per support 50 kN/mm, ballast damping (loss factor) 1, half sleeper mass 162 kg, sleeper spacing 0.6 m and rail type 60E1. Fig. 4 shows a sketch of the track model. Fig. 5 shows five of the receptances taken on the track span (32, 40, 44, 52 and 60 cm from the support) from among the total of 15 (spaced 4 cm apart) that were studied. It can be seen that there are some major differences between the receptances on different sections of the track span, especially at frequencies close to the so-called pinned-pinned resonance frequency.

2.2. Wheelset model

Only one-half of the wheelset is modelled, and it is considered as a lumped mass (M_w) of 600 kg at the centre of gravity of the wheel. In the case under consideration, the static weight (W) of the vehicle that this wheel is supporting is 100 kN. The equation of the model is given in Eq. (4):

$$M_w z_w'' + f_c = W \tag{4}$$

where z_w'' is the second time derivative of the vertical displacement of the wheel.

2.3. Wheel-rail contact

The wheel-rail contact force is calculated using a non-linear Hertz contact spring, which is proportional to the compression of the Hertz spring in the contact between the wheel and rail to the power of 3/2. The Hertz spring constant [21] is $C_H = 93.7$ GN/m$^{3/2}$.

$$f_c = C_H (z_w - z_r - r)^{3/2} \quad \text{when } z_w - z_r - r \geq 0 \tag{5}$$

$$f_c = 0 \quad \text{when } z_w - z_r - r \leq 0$$

where z_w is the vertical displacement of the wheel and z_r is the vertical displacement of the point on the rail in contact with the wheel. The value of r in Eq. (5) is the trajectory of the centre of the wheel resulting from the movement over the defect, considering the shape of the defect and also the wheel curvature. The value of r was calculated in accordance with [27].

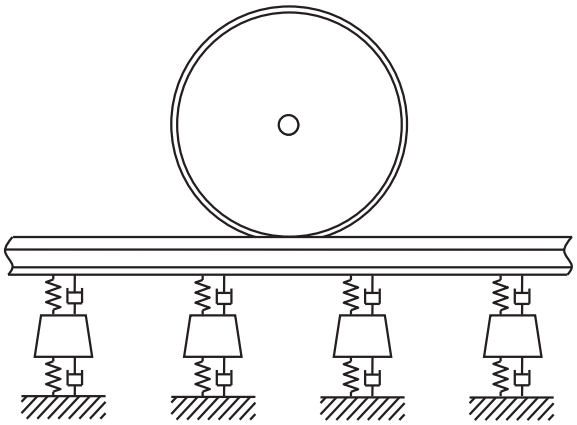

Fig. 4. Sketch of the track model.

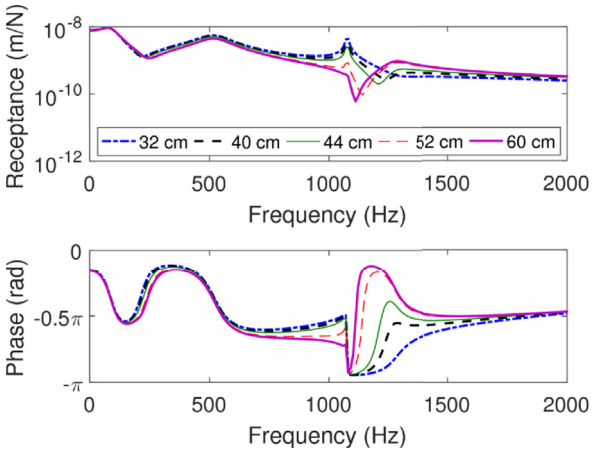

Fig. 5. Track receptances on the 32, 40, 44, 52 and 60 cm track span sections.

2.4. Validation of the model

This section shows validation of the model for a defect at the wheel-rail contact using experimental results obtained by Johansson [28]. In Ref. [28], the authors measured the maximum values of the contact force over a rail for a wheel with wheel flat $d = 0.9$ mm amplitude and length $L = 0.1$ m. The shape and dimensions of the wheel flat defect are represented in Fig. 6 (in continuous line), where x is the coordinate along the rail. This wheel flat defect is expressed as a cosine function with wavelength L, where the full wave amplitude is d. The value of r is shown in dashed line in Fig. 6.

The track parameters are set out in Ref. [30] and are as follows: pad stiffness 120 kN/mm, pad damping 16 kNs/m, ballast stiffness per half sleeper 140 kN/mm, ballast damping per half sleeper 165 kNs/m, sleeper mass (half) 125 kg, sleeper spacing 0.65 m, rail 60E1, static preload 118 kN, half the wheelset mass 593 kg and wheel radius 0.45 m. The track was fitted to these parameters, and the forces during the ride were simulated.

Fig. 7 shows the experimental results obtained by Johansson [28] for the passage by a wheel with the wheel flat mentioned previously. The blue dots represent the maximum values of the contact forces, which were measured experimentally. The results obtained using this model for this track are shown in red. Specifically, the region between the upper and lower envelope curves represents the maximum contact forces for the different positions along the span where the wheel flat makes contact with the rail. A thicker red line indicates a greater difference in the contact forces obtained for the different positions where the wheel flat makes contact with the rail.

As shown in Fig. 7, the results obtained experimentally by Johansson and those obtained in this paper are quite similar, producing a good fit between the results of the present model and the points representing Johansson's experimental values.

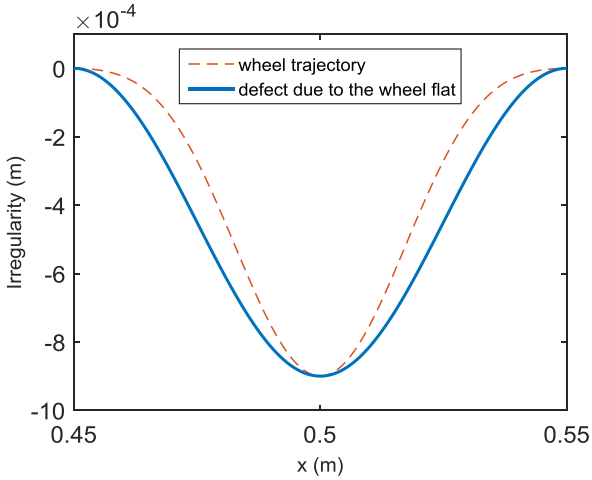

Fig. 6. Shape of the defect due to the wheel flat used in Refs. [29,30] (in continuous line) and the trajectory of the centre of the wheel (in dashed line).

Fig. 8 shows a comparison between the numerical results obtained by Pieringer et al. [30], using a model based on Green's functions as in Refs. [33,34], and those obtained using this model for a wheel flat with different amplitudes and lengths (interrelated). This comparison was carried out to study the validity of the quasi-stationary approach of the present model for high train speeds. This figure shows only the results corresponding to greater values of the maximum contact force for different contact positions between the wheel flat and the track. These results are shown up to speeds of 300 km/h, with excellent concordance between the two models.

3. Parametric study of contact forces when passing over rail welds

In this section, the interaction model that was described and validated previously is used to obtain the contact forces produced when vehicles move over rail welds. These welds may act as surface defects, and depending on their shape and severity, these defects can lead to large contact forces that may even cause loss of contact and heavy impacts.

To accomplish this study, several rail weld profiles measured by Steenbergen and Esveld [1–3] and other measured in the vicinity of Bilbao were used as initial input.

The results shown in this section were obtained based on the weld defect shown in Fig. 9, which was taken from the study by Steenbergen [2].

Fig. 10 shows a 3D graph of the maximum contact forces when a vehicle moves over the rail weld shown in Fig. 9, as a function of speed and weld position. The sleepers are located at 0 cm and 60 cm. Here, the non-linearity of these forces may be observed, as already shown by the authors [25]. For every position of the weld along the span between two sleepers, it will be noticed that the contact force increases with speed up to 80–100 km/h, and with further increase in speed, the contact force decreases considerably.

This decrease takes different values depending on the position of the weld along the span. Specifically, if the weld centre is located 10–30 cm after the sleeper, an abrupt decrease in the maximum contact forces occurs at speeds close to 80 km/h, whereas this decrease is gradual for other positions of the weld along the span.

In order to understand this non-linear behaviour of wheelset-rail dynamics when vehicles move over rail welds, a detailed study was carried out on the contact force changes in the time domain for each wheelset speed. Fig. 11 shows, against train speed, the maximum contact force for a rail weld centred 15 cm after the sleeper. The bottom section of Fig. 11 shows the development of contact forces in the space domain, for the speeds indicated with capital letters in the upper section of the figure. For example, the contact force in the space domain corresponding to point A (55 km/h) in the upper section of the figure is shown in the first graph in the lower section of the figure. At this low speed, it is already possible to observe the fluctuation in the contact force due to the movement over the rail weld. Between speeds of A and B (80 km/h), the contact force increases up to a relative maximum at B. At speeds above B, it may be observed how the contact force that was initially a single peak begins to split into two (see C, 150 km/h), reducing the maximum value of the contact force. As may be observed, the second of the two peaks is of a greater magnitude than the first. This new peak starts increasing progressively, as may be observed at D (170 km/h). If the speed continues to increase, the first peak again becomes the maximum peak and continues to rise up to 200 km/h.

In order to interpret this result, the relationship among the contact forces, weld defect, and displacements of the wheelset and rail, is analysed. Fig. 12 shows the contact forces and the displacements of the wheelset and rail as the vehicle moves over the weld shown in Fig. 9. The subfigures labelled (a) in Fig. 12 show the forces on the contact (unbroken line) between the wheelset and rail, as in Fig. 11, although the weld defect is shown superimposed on the contact force (broken line). The subfigures labelled (b) show the displacements of the wheelset (in red) and the displacements of the upper point on the rail surface (in blue), where contact is made. These forces and displacements are represented for the following speeds: 20 km/h

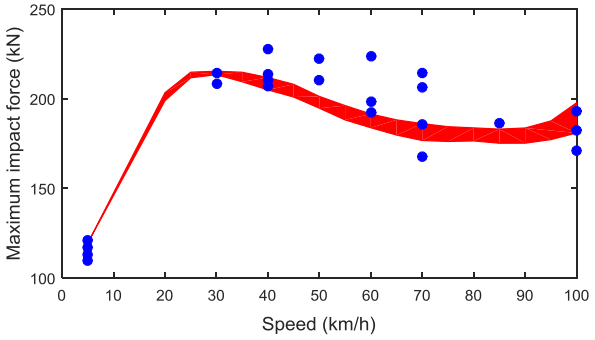

Fig. 7. Validation of the method with the experimental results of Johansson and Nielsen [28]: results of the model used in this paper (in red) and the experimental results of Johansson and Nielsen (blue dots). (For interpretation of the references to colour in this figure legend, the reader is referred to the web version of this article.)

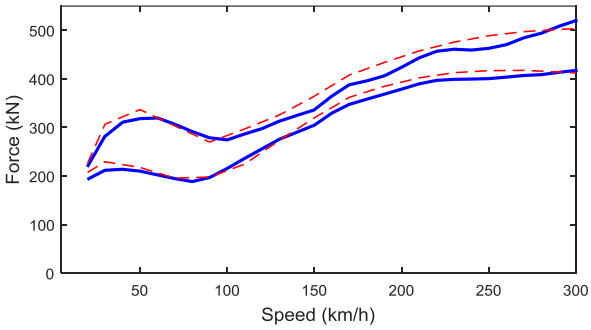

Fig. 8. Validation of the method with numerical results obtained by Pieringer [30] for rounded wheel flat defects with amplitudes of 1 and 2 mm. The results obtained by Pieringer are shown as continuous lines, whereas the results obtained using the present model are represented as dashed lines.

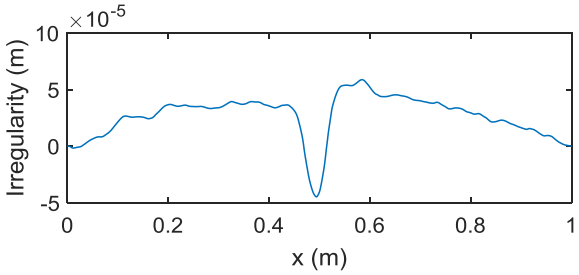

Fig. 9. Weld defect profile 1 (from Steenbergen [2]).

(O), 55 km/h (A), 80 km/h (B), 150 km/h (C), 170 km/h (D) and 200 km/h (E). The last five speeds match the points A, B, C, D and E in Fig. 11. The weld defect is centred at centimetre 15 on the span for all of these figures.

At low speeds, as shown at O (20 km/h), it may be observed that both the wheel and the rail follow the irregularity very closely. Only a slight discrepancy is observed between the position of the defect and the response of the wheel and the rail. The compression of the Hertz spring between the wheel and rail still remains practically constant as the train moves over the weld dip, and therefore, the contact force as it moves over the weld is practically unchanged.

When the running speed increases (see A and B), it may be observed that the discrepancy between the weld and the response of the wheel and the rail is increasingly greater. Moreover, both the wheel and the rail have a smaller descent in the area containing the weld dip. As the running speed increases, the wheel increasingly ceases to follow the irregularity due to its high inertia, and the wheel suddenly discharges when it reaches the dip in the weld. Due to this discharge, the descent in the rail also diminishes. This is why the point on the rail surface descends less when the running speed increases. At 55 km/h (A),

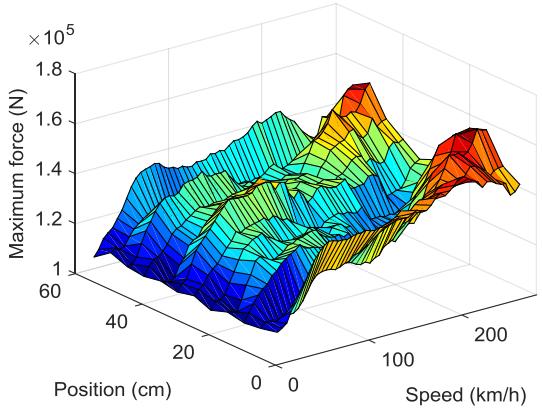

Fig. 10. Maximum contact force against the relative position of the weld with respect to the sleeper and against the speed, when the vehicle moves over the rail weld defect shown in Fig. 9.

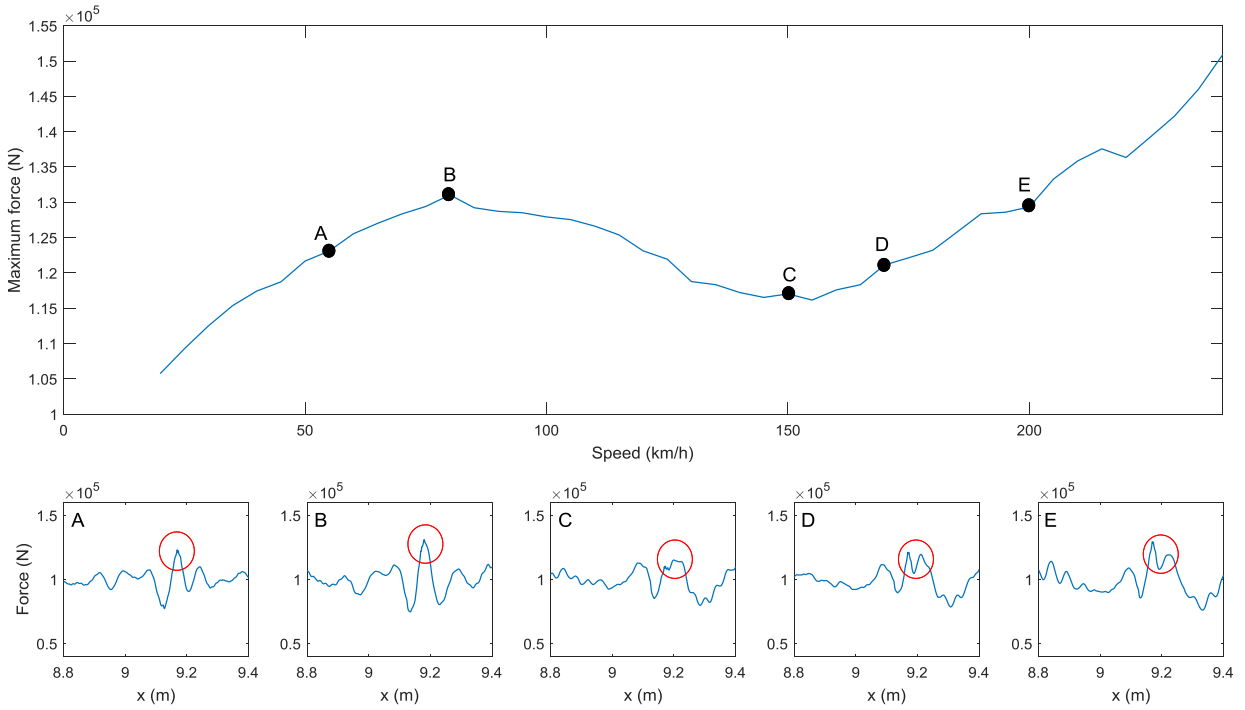

Fig. 11. Above: Influence of speed on the maximum contact force, when the rail weld is centred 15 cm after the sleeper. Below: Contact forces in the space domain when a vehicle moves over the rail weld, for different speeds: (A) 55 km/h, (B) 80 km/h, (C) 150 km/h, (D) 170 km/h, (E) 200 km/h.

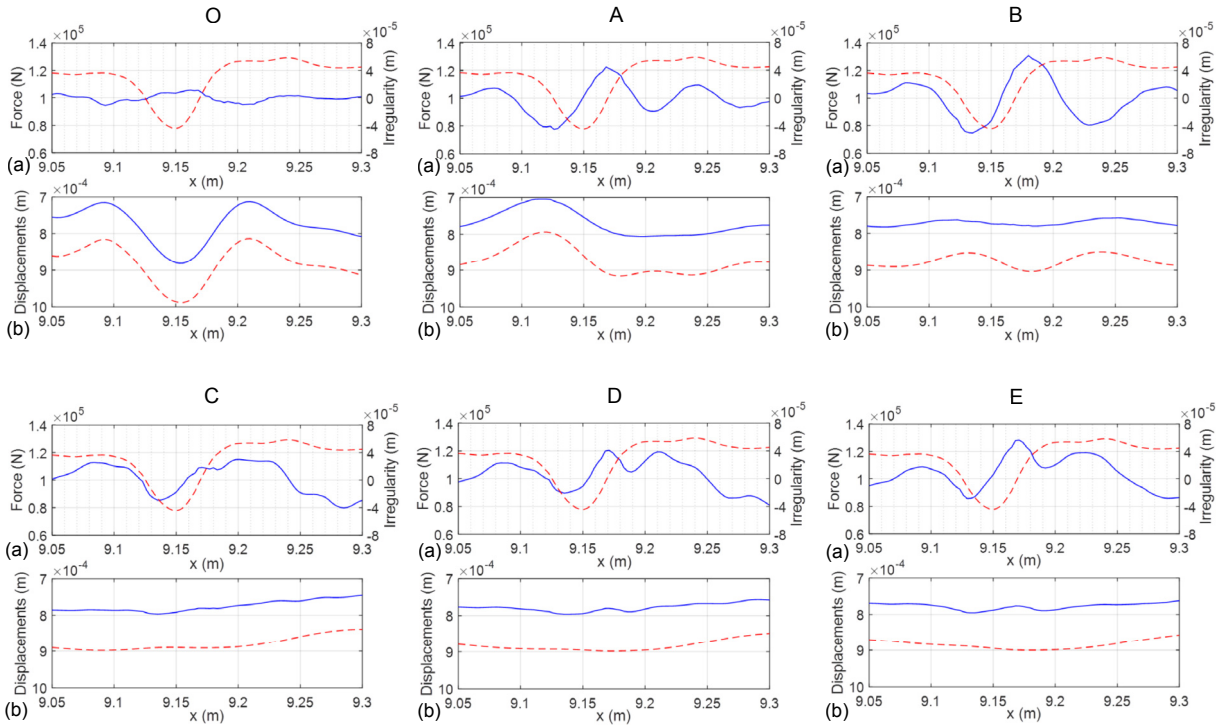

Fig. 12. Contact forces and weld defect (a) and displacements of the wheel and the rail (b) as the vehicle moves over the weld shown in Fig. 9, for the following speeds: (O) 20, (A) 55, (B) 80, (C) 150, (D) 170 and (E) 200 km/h.

it may be observed that the contact forces show substantial variations as the train moves over the weld, with the peak of the force located on the upward ramp of the dip in the weld, roughly at the point of inflection of curvature on the upward ramp.

At approximately 80 km/h (B), the maximum peak of the contact force starts to move slightly to the right. This is because the maximum descent of the wheel also moves to the right, as it is subject to substantial inertia. The relative maximum value of the contact force, i.e. the speed at which the compression of the Hertz spring between the wheel and rail is greatest, is produced at speeds close to 80 km/h.

Beyond 80 km/h, the maximum peak of the force begins to split into two, as may be observed at 150 km/h (C) and 170 km/h (D). At 170 km/h, it may be observed that the rail starts to rise at around 9.18 m, whereas the vertical displacement of the wheel remains almost the same. This is consistent with what is shown in Ref. [26] for the case of wheel flats. This behaviour is due to the vibration of the rail itself, and it causes the appearance of the second of the two peaks in the contact force. Beyond 170 km/h, it may be observed that the descent of the wheel as it moves over the weld dip is very small in the weld area. As the displacement of the wheel is negligible in the area around the defect, the fluctuation in the contact force is caused by the fluctuation of the rail descent, as shown in the figure.

This is an interesting result, as it would reveal, for a certain type of track, the positions of the rail weld along a span between two sleepers at which the maximum contact forces would be more severe when the vehicle moves over the weld. This could eliminate any unfavourable positions for welds during the track construction process, and plans could be made in advance for preferential locations, in order to reduce the maximum contact forces. For the case studied, it is evident that there is some advantage in locating the welds 10–30 cm after a sleeper, where a large hollow arises in the maximum contact force for train speeds between 120 and 200 km/h, which is a considerable speed range. Besides, another advantage for this defect position is that an increase in train speed beyond that interval would not cause an increase in maximum contact forces, which could even decrease as has been shown.

It is also interesting to note how the contact forces vary due to the parametric excitation caused by the discrete support on the sleepers, even if there is no weld on the rail. This is shown in Fig. 13. The points 16.8, 17.4 and 18 on the x-axis correspond to positions over the sleeper. It may be observed in the figure that the contact force fluctuates around its mean value (in this case 100 kN) as mentioned previously, due to the sleeper passing frequency and its harmonics. It also shows that the peaks of this fluctuating component of the force move towards the right as the speed increases. This displacement is shown as the shaded area in Fig. 13.

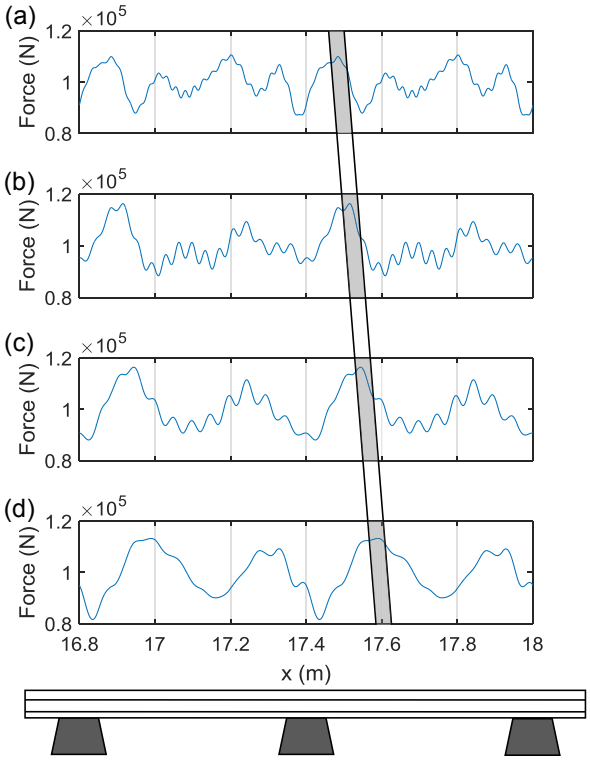

Fig. 13. Contact force due only to the parametric excitation in the absence of a weld defect, for different running speeds: (a) 100 km/h, (b) 150 km/h, (c) 200 km/h and (d) 250 km/h.

4. Generalisation of the study of contact forces for other types of weld defects

This section extends the previous study to other types of weld defects. More than 500 welds were measured experimentally and studied, and the following classification was established: welds that have a dip as the main characteristic, and welds that have either no dip or the dip is secondary with respect to the presence of a protrusion having an amplitude much larger than that of the dip.

4.1. Weld defects with a dip

A study was conducted on the maximum forces when the wheel passes over rail welds with profiles as shown in Figs. 14 and 15, which were taken from the studies by Steenbergen and Esveld [1,3].

For rail welds of the same type as these, it was observed that the behaviour of the dynamic system is very similar to what was studied in the previous section, even though the shape of these types of rail welds is quite different to that shown in Fig. 9. While the distinguishing feature of the weld in Fig. 9 was a dip in the central region, the weld in Fig. 14 contains a superelevation in the central region, but with shrinkages at both sides, and the first dip, which is close to cm 47, is larger. Even though it has both a protrusion and a dip, the effect of the dip will prevail over the effect of the protrusion in terms of the tendencies in the maximum force, because the dip and the protrusion are similar in size. This is why it was classified in the group of weld defects with a dip. As shown in Fig. 16, the shape of the 3D plot of the maximum contact force against speed and against weld position are very similar to those shown in Fig. 10, although the relative minimum contact forces appear at other speeds. In this case, it is also evident that the dips have very similar values of maximum contact force among all the sections in a span between two sleepers. However, the lowest values of these maximum contact forces appear for the weld defect position centred 40 cm after the sleeper, at speeds between 80 and 250 km/h. At 40 cm, however, the force becomes minimal only in this range, with very high values at lower speeds. On the other hand, at around 25 cm, the maximum force is quite small at all low and medium speeds, making this a better location for the weld.

Fig. 17 again shows the maximum contact force against the relative position of the weld with respect to the sleeper and against the speed when the vehicle moves over the rail weld defect shown in Fig. 15. Again, this rail weld has a dip in the central zone; however, in this case, it is much longer than in the previous dip, coinciding with the ground area around the weld. As a result, it has two protrusions at the initial and final areas of the weld, but the dip has a greater effect. In this case, for speeds above around 250 km/h, a loss of contact occurs. In this case, it is possible to distinguish also two dips around 120 km/h (slight) and around 250 km/h. Moreover, the contact forces when the rail weld is located in the first 15 cm after the sleeper are considerably lower than when it is located elsewhere.

Therefore, it is concluded in this Section that, in general, when the weld defect has a dip, the behaviour when the train moves over different types of welds is similar, although the weld defects themselves have very different shapes. In all the cases that were studied, it was confirmed that the maximum wheel-rail contact force does not increase linearly with running speed. On the contrary, it was observed that for the different positions of the weld, it is possible to find an interval of running speeds in which the maximum contact force remains almost constant or even decreases.

This result totally concurs with the experimental field measurements on a real track by Johansson and Nielsen [28], which were conducted to study the contact forces due to wheel flats. In terms of contact, these wheel flats are equivalent to having a relative dip between the wheel and rail, in such a way that the centre of gravity of the wheel approaches the rail. The size of the wheel flat defect is also in the order of a few centimetres. Therefore, this defect is similar to the weld defects studied here. Johansson and Nielsen confirmed with their measurements of wheel passage forces for increasing running speeds that the curve of maximum force against speed increased up to a certain value of speed, reached a relative maximum, and subsequently decreased. Pieringer [30], with her numerical model, found that if the running speed continued to increase further, the maximum contact force reached a minimum, and afterwards the contact force started to increase again with the speed. Therefore, although the defect from the wheel flat is more severe, this defect and those in the rail welds of the types studied in both this section and the previous section lead to very similar increasing tendencies for the maximum contact forces with respect to speed.

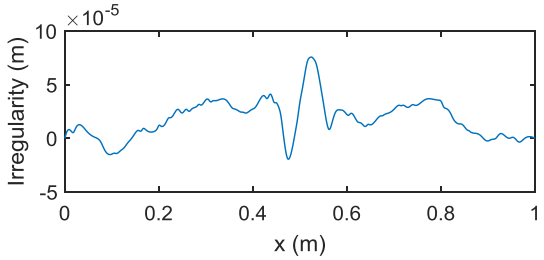

Fig. 14. Shape of weld defect 2 (Steenbergen and Esveld [1]).

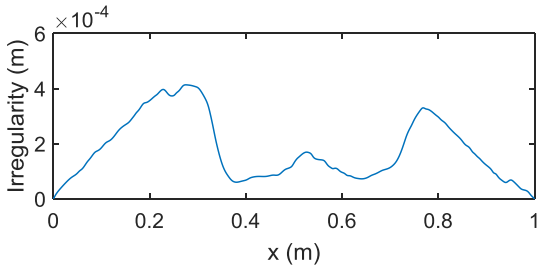

Fig. 15. Shape of weld defect 3 (Steenbergen and Esveld [1,3]) (aluminothermic weld).

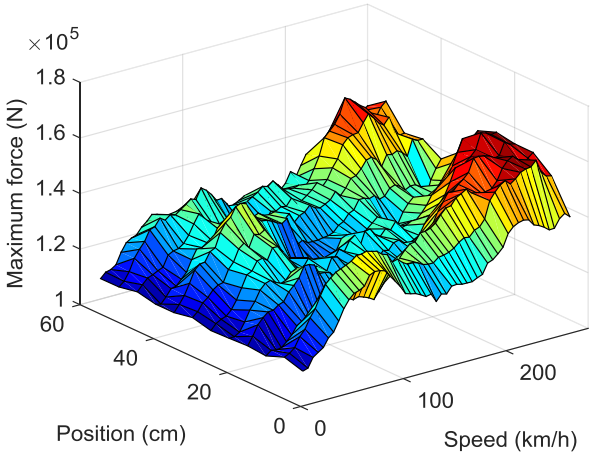

Fig. 16. Maximum contact force against the relative position of the weld with respect to the sleeper and against the speed, when the vehicle moves over the rail weld defect shown in Fig. 14.

4.2. Weld defects with a protrusion and no dip, or with a dip that is negligible compared to the protrusion

Contact forces do not have the same pattern of behaviour for all types of rail welds. In this section, two more types of rail welds will be studied: one taken from the study by Steenbergen and Esveld [1] (Fig. 18) and the other from a renewed line in the vicinity of Bilbao (Fig. 19).

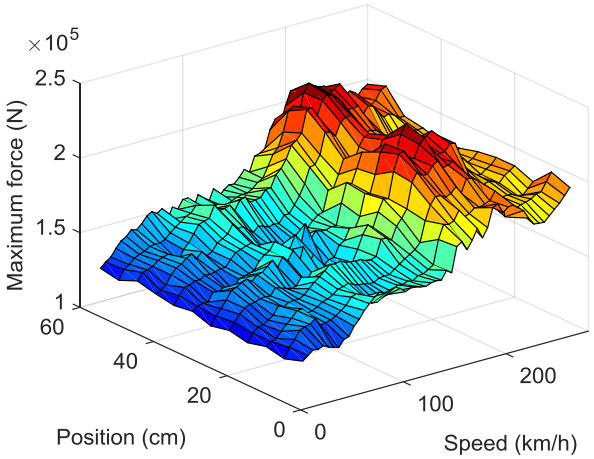

Fig. 17. Maximum contact force against the relative position of the weld with respect to the sleeper and against the speed, when the vehicle moves over the rail weld defect shown in Fig. 15.

Fig. 20 shows the 3D plot of the values of the maximum contact force against the relative position of the weld with respect to the sleeper and against the speed, when the vehicle moves over the rail weld defect shown in Fig. 18. The main feature of this weld is that it acts on the wheelset-rail interaction as a ramp with a high slope. Large impacts are thus produced. For this type of defect, it may be observed that the maximum force varies in a virtually linear manner with respect to the speed of the wheel over the defect. This is in contrast to the effect produced by the defects containing a dip, which have been shown in the paper so far. The reason for such a different tendency compared to previous cases is the shape of the defect itself. For example, in the weld shown in Fig. 9, there is a dip at the centre of the weld, whereas the main characteristic of the weld shown in Fig. 18 is the upward ramp at the beginning of the defect. The maximum force in this type of defect is in fact caused by the interaction with the upward ramp, which causes the maximum force to increase linearly with speed.

It may also be observed that the influence of the weld defect is very high, when compared to that of the parametric excitation, and the fluctuations of the forces caused by the presence of the weld are dominant with respect to the fluctuations in the force caused by the movement over the sleeper. As a result, the contact forces increase with speed quite independently of the position of the weld defect.

Fig. 21 shows the 3D plot of the maximum contact force against the relative position of the weld with respect to the sleeper and against the speed, as the vehicle moves over the rail weld defect shown in Fig. 19. In this case, it is observed that the maximum contact force increases almost linearly with speed. This same tendency can be observed for almost all positions of the weld defect within the span between two sleepers. The explanation for this again lies in the shape of the defect. Although the defect also has a number of dips at the centre of the weld, they are not very significant compared to the protrusion, because of the upward ramp located at the beginning of the defect. At the beginning of the ramp, the contact force increases considerably, and reaches its maximum value approximately three quarters of the way up the ramp, followed by a discharge. The contact force again increases on the protrusion at the centre of the weld; however, this increase is less than that at the beginning of the weld.

In this weld, it may be observed that the values of the maximum force-speed curve are different for different positions of the weld defect. This is due to the effect of parametric excitation, which is not negligible for this defect, since the defect does not have such a large amplitude. If the amplitude of the defect were larger, the effect produced by the movement over the sleeper would have diminished, in such a way that this 3D graph would be practically flat, as in the preceding case.

Therefore, it may be concluded that the shape of the 3D plot of contact forces against speed and position in the span between two sleepers will not be similar for every type of weld. In fact, it has been demonstrated that among the five types of weld shown, only three of them show hollows in the plot for certain speed ranges and/or weld positions (welds in Figs. 9, 14 and 15). Besides, other types have been found (Figs. 18 and 19) in which the defect impact is so important in comparison to the other factors that the increase in maximum forces with speed is almost linear.

5. Influence of the discrete support on maximum contact forces during passage over welds

As mentioned above, the discrete support of the track is most important to the shape of the 3D graphs of the maximum force-speed-position of defect for some of the welds that were analysed. The influence of the discrete support of the track manifests itself in different ways in the maximum contact forces as the vehicle moves over the weld defects. All these manifestations are due to the changes in the stiffness of the track at the position of contact with the wheel.

The position of the weld defect can completely change the contact force, and the way in which contact forces evolve as the running speed increases.

Before the wheel reaches a defect, the wheelset-rail contact force is already fluctuating slightly. This is solely due to the variations in stiffness, due to the contact with the various points along the span. This can be seen in Fig. 13. This component of the force caused only by the wheel moving over the points on the rail with variable receptance is responsible for a significant part of the fluctuation in the maximum force at different positions of the weld along the track span. As an example, Fig. 22a shows the maximum value of the dynamic component of the contact force, at different positions and at different speeds, as the vehicle moves over the weld shown in Fig. 9. This result was presented above in Fig. 10, with the difference that in Fig. 22a the value of the static component of the contact force has been subtracted. Fig. 22b shows the maximum values of the difference between the contact force as the vehicle moves over the weld and

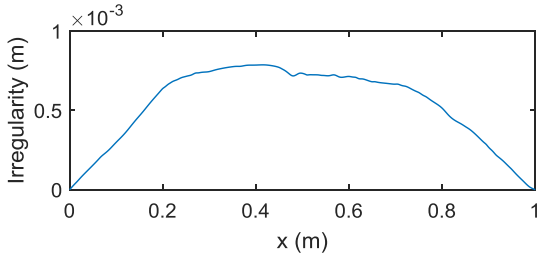

Fig. 18. Shape of weld defect 4 (Steenbergen and Esveld [1]).

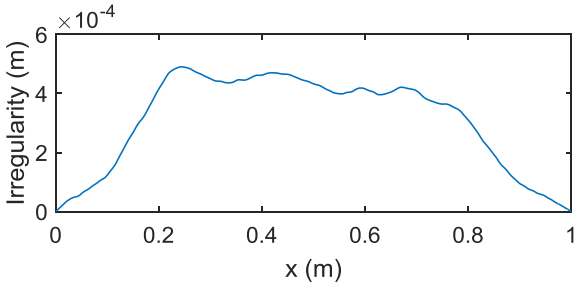

Fig. 19. Shape of weld defect 5 (aluminothermic weld).

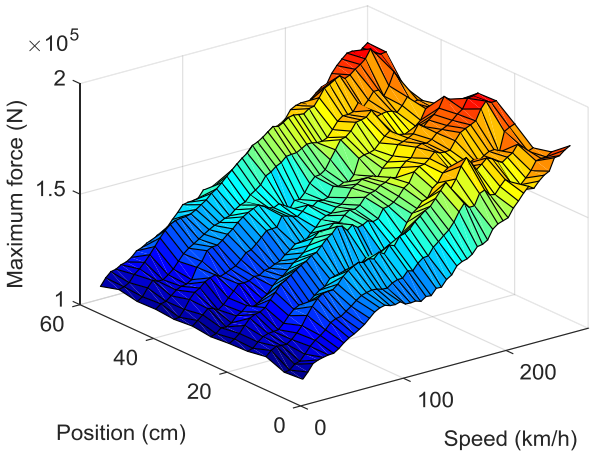

Fig. 20. Maximum contact force against the relative position of the weld with respect to the sleeper and against the speed, when the vehicle moves over the rail weld defect shown in Fig. 18.

the contact force that would have been obtained if the rail had been perfectly smooth (with no weld defect). These two graphs are superimposed in Fig. 22c for comparison. It may be observed that most of the 3D surface hollows in Fig. 22a disappear in Fig. 22b, as the value of the force without any weld has been subtracted. For some positions of the weld on the span, the values are greater in Fig. 22a. This relates to situations in which, at the position of the maximum peak of force as the vehicle moves over the weld, the force produced by the movement of the wheel over the smooth rail was greater than the static force. It may be observed that the surface in Fig. 22b is much smoother, and that the differences in

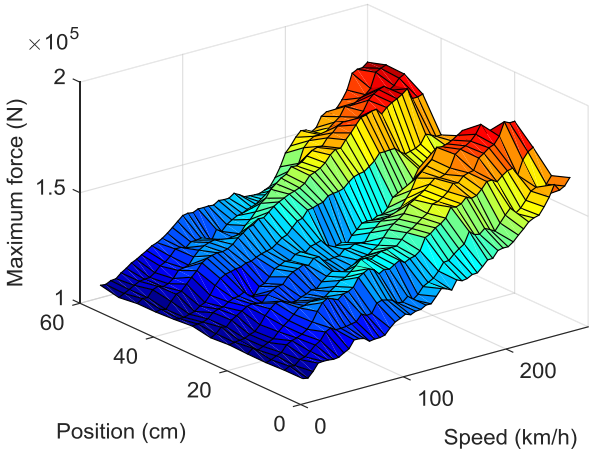

Fig. 21. Maximum contact force against the relative position of the weld with respect to the sleeper and against the speed, when the vehicle moves over the rail weld defect shown in Fig. 19.

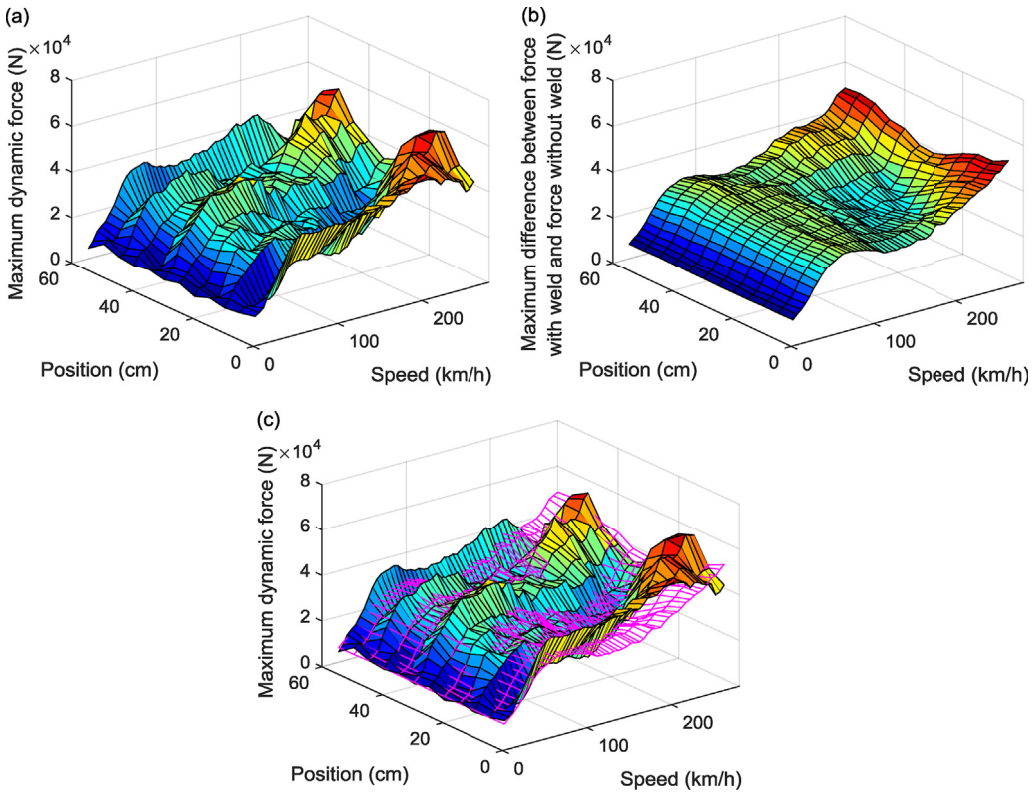

Fig. 22. (a) Maximum dynamic contact force when the vehicle moves over the rail weld defect shown in Fig. 9. (b) Maximum increase in the contact force when the vehicle moves over the rail weld defect shown in Fig. 9 with respect to the force when there is no weld. (c) Comparison between the surfaces in (a) and (b).

values for different positions of the weld on the span are much smaller, although there are still differences among the weld positions. This is because the effect of the change in stiffness of the various positions on the track span still contributes to the contact force value resulting from the presence of the weld, as observed in Fig. 22b. Not all the hollows in Fig. 22a disappear – the hollow for speeds between 120 km/h and approximately 200 km/h is maintained, especially when the weld is centred between centimetres 15 and 35 on the span. Moreover, the highest values of the increase in force with respect to a smooth-rail scenario arise when the weld is centred in areas around the sleeper.

6. Influence of the length and wavelength content of the defect, contact stiffness and frequency content of the wheelset-track system on tracks with continuous support

In order to simplify the study carried out in this section and to draw conclusions more directly, a track with continuous support was used. This track has a similar receptance (up to approximately 800 Hz) to that of the track whose parameters are described at the end of Section 2.1. This eliminates the effect of parametric excitation over different sections of the track, with no changes to the amplitudes or frequencies of track receptances over a wide range of frequencies.

6.1. Effect of the length of the defect and the stiffness of the Hertzian contact spring

In order to study the influence of the length of the defect, the contact forces on a track with continuous support, as described above, were obtained.

It was observed that doubling the length of a given defect on the rail surface and maintaining its amplitude displaces the hollows on the curve, thus showing maximum force against speed. Doubling the length of the defect and maintaining its amplitude logically displaces the relative maximum on this curve, in such a way that the relative maximum emerges at approximately twice the speed. An example of this is shown in Fig. 23, which shows the maximum force/speed curves for the track with continuous support, for two defects with the same cosine function shape and same amplitude (40 μm) but different wavelengths (48 and 96 mm respectively). The shape of this defect for a length of 48 mm is shown in Fig. 24. This type of defect has been chosen as a benchmark defect to study welds with a dip. A particularly small defect amplitude was taken in order to determine the way in which the maximum force curve changes with speed, even for a defect with a very small amplitude. The curves are of the same shape; however, in the curve for the weld with a 48 mm

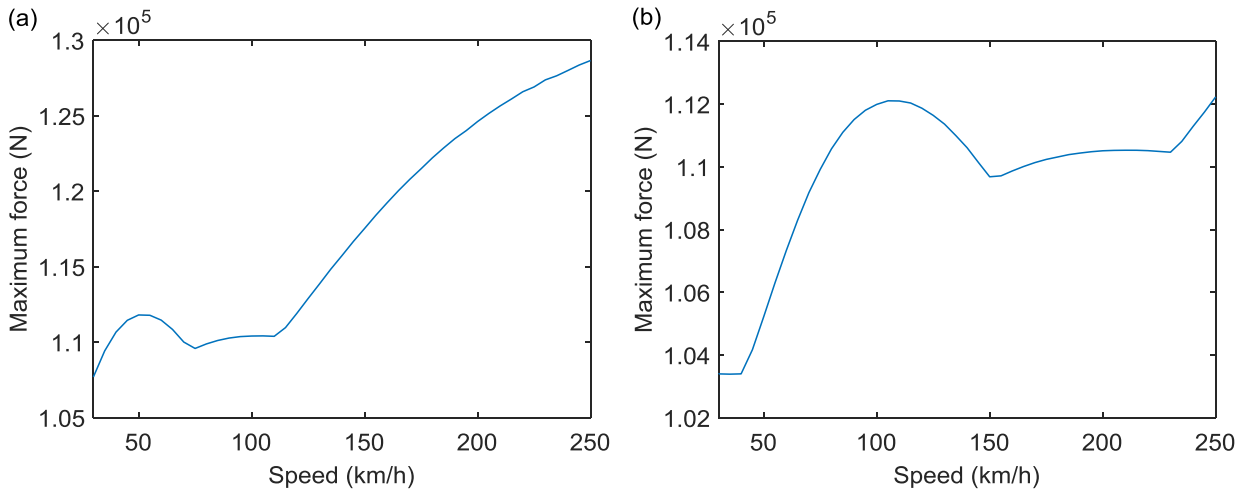

Fig. 23. Effect of speed on the maximum contact force when the vehicle moves over: (a) a weld with a wavelength of 48 mm (shown in Fig. 24) and (b) a weld with a wavelength of 96 mm.

wavelength, the speed at which the curve reaches its maximum is approximately 53 km/h, whereas when wavelength is 96 mm, the speed at which the maximum is achieved is approximately 107 km/h (i.e. approximately twice the speed shown on the 48 mm wavelength graph). This is consistent with the results shown in Ref. [26] for the case of wheel flats, where it was observed that the relative maximum in the maximum force/speed curve shifts towards higher speeds as the wheel flat length increases.

Fig. 23 shows sharp angles at 74 and 112 km/h (in Fig. 23a) and at 152 and 230 km/h (in Fig. 23b). When the maximum is reached on the curve, a division of the peaks in the contact force may be observed. For this defect, one of the peaks emerges on the upward ramp of the weld dip, and another one emerges slightly further away. At 74 km/h, in the case of the 48 mm wavelength (or 150 km/h in the case of the 96 mm wavelength), the peak of the force showing a greater amplitude is overtaken by the other peak, and this creates the sharp angle. Similarly, at around 112 km/h in the case of the 48 mm wavelength (or 230 km/h in the case of the 96 mm wavelength), another change occurs in the maximum peak, and another sharp angle appears.

It is perceived that this has a very similar effect to decreasing or increasing (to scale) the frequency of the track. Frequency escalation goes beyond merely changing the length of a defect, because escalation should also be carried out on the rest of the mechanical system. However, as already mentioned, the vibration of the rail exerts the dominant effect on this type of welds with a dip, and the track almost completely dominates the division of the force peaks. Therefore, the track determines the speed at which the maximum point on the maximum force/speed curve is reached, as shown here.

A study was conducted on the effect of stiffness of the Hertzian contact spring. It was observed that this affects the maximum force/speed curve by increasing or decreasing the maximum value of the contact force, without changing the shape of the curve. Changing the stiffness of the Hertzian contact spring from 50×10^9 to 100×10^9 N/m$^{3/2}$ causes a change in the maximum contact force of approximately 10% of the nominal value of the force. Nevertheless, when the contact stiffness increases, a slight displacement is observed towards higher speeds on the relative maximum of the curve. This means that the separation between the peaks of maximum force, when the vehicle moves over the weld, occurs at higher speeds as contact stiffness increases. This pattern of behaviour caused by the change in contact stiffness was observed for various types of welds (with dips and with protrusions).

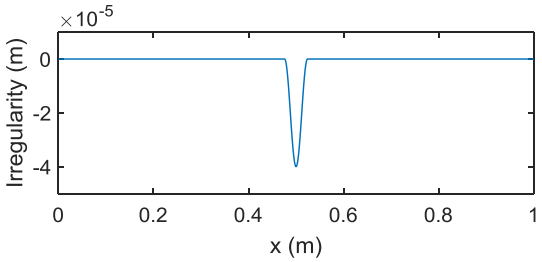

Fig. 24. Weld defect with a cosine function dip with a 48 mm wavelength.

6.2. Effect of frequency components of the wheelset-track system and the weld defect

This section examines the frequency components of the force, the track-vehicle system and the weld itself (corrected to take into account the wheel shape/curvature). In order to simplify the study on the effect of the receptances of the wheelset-track system, again a track with continuous support was used.

6.2.1. Study in the frequency domain

This subsection performs an analysis on the influence of the various frequency components of the wheelset-track system and the weld itself.

Fig. 25A shows the FFT of the contact forces on the track with continuous support, as the wheel moves over the weld shown in Fig. 9 with varying running speeds. Fig. 25B shows the FFTs of the weld irregularity, also at different speeds. Fig. 25C to F show the receptances of the wheelset-track system superimposed over the FFT of the contact forces (above) and the FFT of the weld irregularity (below) at speeds of: 55 km/h (C), 120 km/h (D), 145 km/h (E) and 220 km/h (F). The wheelset-track receptance shows two peaks at frequencies of 60 and 240 Hz. These FFTs are all shown in the frequency domain and not in the wavelength domain. The peaks of the irregularity FFT, however, do not occur at constant frequency, but rather at constant wavelength. This causes the peaks of the irregularity FFT to displace in a linear fashion with the speed of the wheelset. The resonances of the wheelset-track system, on the other hand, do not show any displacement with speed.

Fig. 25 shows that, logically, the contact force FFT contains practically the same frequency components as the irregularity at each speed. Fig. 25C to F show that, when the speed increases, the force FFT follows the irregularity FFT.

The distribution of energy over the peaks of the contact force FFT, however, is not maintained at all speeds. It is observed that when a certain defect frequency component coincides with one of the resonant frequencies of the wheelset-track system (in this case 60 and 240 Hz), the energy content of the force at that frequency increases considerably.

As an example, at 55 km/h (C), the 25 cm wavelength component of the irregularity, which at this speed corresponds to a frequency of 60 Hz, excites the vehicle-track system at this frequency of approximately 60 Hz (see Fig. 25C), which coincides with the frequency of the first peak of the receptance of the wheelset-track system. The coincidence of these two frequencies leads to a major increase in the amount of energy shown by the contact force at this frequency.

At 120 km/h (D), a large peak in the contact force FFT occurs again at 60 Hz, corresponding to a wavelength of 55 cm for this speed. Again, the coincidence of the 60 Hz frequency of receptance of the wheelset-track system with the 60 Hz frequency of the irregularity excites this frequency component of the force. At 145 km/h (E), the largest peak occurs at approximately 245 Hz, coinciding with a rail defect wavelength of 16.5 cm. At 220 km/h (F), the frequency associated with the 25 cm

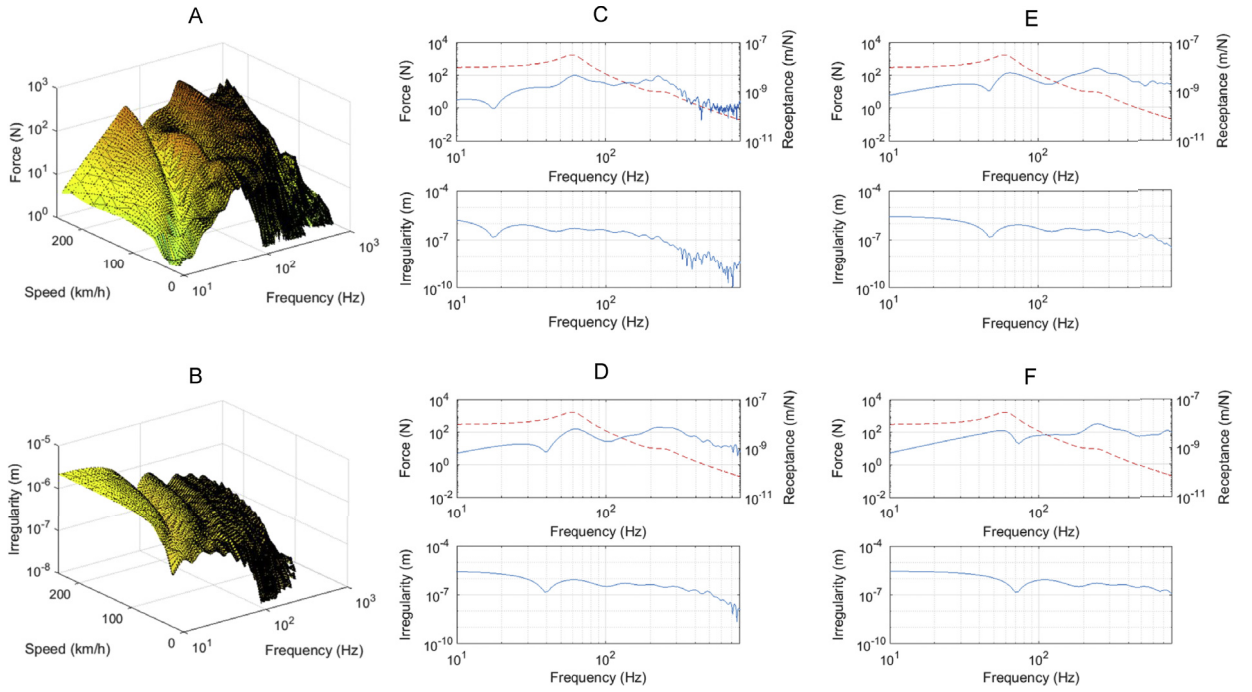

Fig. 25. FFT of the contact force when the vehicle moves over the weld shown in Fig. 9 (A). FFT of the weld defect shown in Fig. 9, depending on speed (B). FFTs of the contact forces when the vehicle moves over the weld shown in Fig. 9 (-) and the receptance of the wheelset-track system (–) (above), and FFTs of the weld shown in Fig. 9 (below), at speeds of 55 (C), 120 (D), 145 (E) and 220 km/h (F).

wavelength is 244 Hz, which is quite close to the resonance frequency of the wheelset-track system (240 Hz). This again causes the amount of energy in this component of the force to rise considerably, as shown in the figure.

It may thus be perceived that the breakdown of the weld into wavelengths has a considerable influence. Moreover, the resonances of the wheelset-track system cause the excitation of a number of frequencies associated with the wavelengths of the irregularity.

6.2.2. Study in the spatial domain

This subsection conducts an analysis to find out why two peaks emerge in the wheel/rail contact force at a certain speed, when that speed increases. The study was carried out using the defect in Fig. 24 (to represent welds with a dip) and another defect with the same shape and dimensions, but inverted to create a protrusion on the rail surface (to represent welds with no dip or with a negligible dip). These two defects of only 40 μm were taken to determine their effect, even with defects with small amplitudes.

As an example, Fig. 26 shows the FFT of the contact force between the wheel and rail at a speed of 120 km/h. It is observed that the first two peaks of the FFT correspond to the resonant frequencies of the track-vehicle system, which are approximately 60 and 240 Hz. However, the components with a greater frequency do not correspond to a track-vehicle resonance, and it was determined that they essentially depend on the weld defect itself. For the purposes of analysis, the dynamic force was divided into two components: a dynamic component with a high frequency, and another component with a low frequency. The low-frequency component was taken as less than approximately 530 Hz, and the high-frequency component was taken as above 530 Hz. This frequency was chosen because it was observed that below 530 Hz the peaks in the FFTs of the forces did not change in frequency. They were therefore associated with the track-vehicle system; whereas above this frequency they moved towards higher frequencies when the speed increased. These FFT peaks are associated with the defect. The high and low frequency components were determined using low-pass/high-pass filtering with a cut-off frequency of 530 Hz. It was ascertained that this separation could be made at all operating speeds. Figs. 27 and 28 show, at different running speeds, the superposition of the total dynamic forces and their high-frequency and low-frequency components, during a wheelset passage over the defect shown in Fig. 24 and over that same defect inverted, respectively.

As a result of what was stipulated above, the low-frequency component shows two FFT peaks at approximately 60 and 240 Hz. It was ascertained that, logically, these frequencies, which do not depend on the defect but relate to the vehicle/track resonance frequencies, may be found in this low-frequency component at any ride speed. The low-frequency component shows hardly any changes to its frequency content with respect to speed; however, the amplitudes of the components may vary at different speeds. It was observed that it is also displaced in the direction of travel when the running speed increases (see Figs. 27 and 28). It may also be observed that the wavelength of this component of the low-frequency force increases linearly with speed, which is logical as the resonant frequencies are constant.

With regard to the high-frequency component of the force, it may be observed that it does not have a constant-frequency composition at any speed. This is because the high-frequency component is associated with the weld defect itself, and therefore, when the running speed changes and the wavelength of the defect remains constant, the frequency composition changes.

The study of the two high-frequency and low-frequency components explains why the maximum contact force decreases when the ride speed increases, as described in previous sections, for defects with dips.

The defect shown in Fig. 24, which has such a dip, was taken by way of example and the results of the total dynamic force when the vehicle moves over this defect and its high-frequency and low-frequency components are shown in Fig. 27.

At low speed (50 km/h), it may be observed that the contact force virtually has only a low-frequency component, whereas the high-frequency component is negligible in comparison to the low-frequency component. The high-frequency component

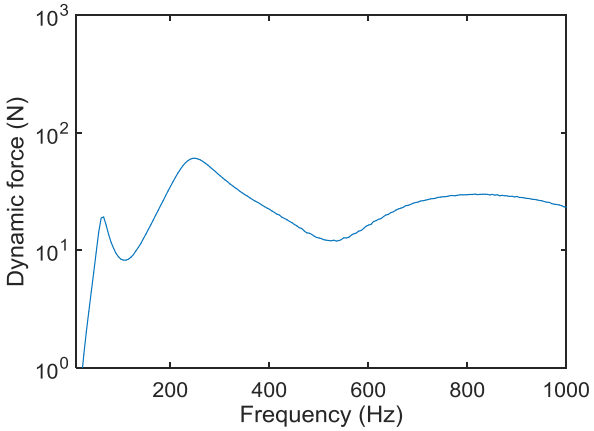

Fig. 26. FFT of the contact force when the vehicle moves over the defect shown in Fig. 24, at 120 km/h.

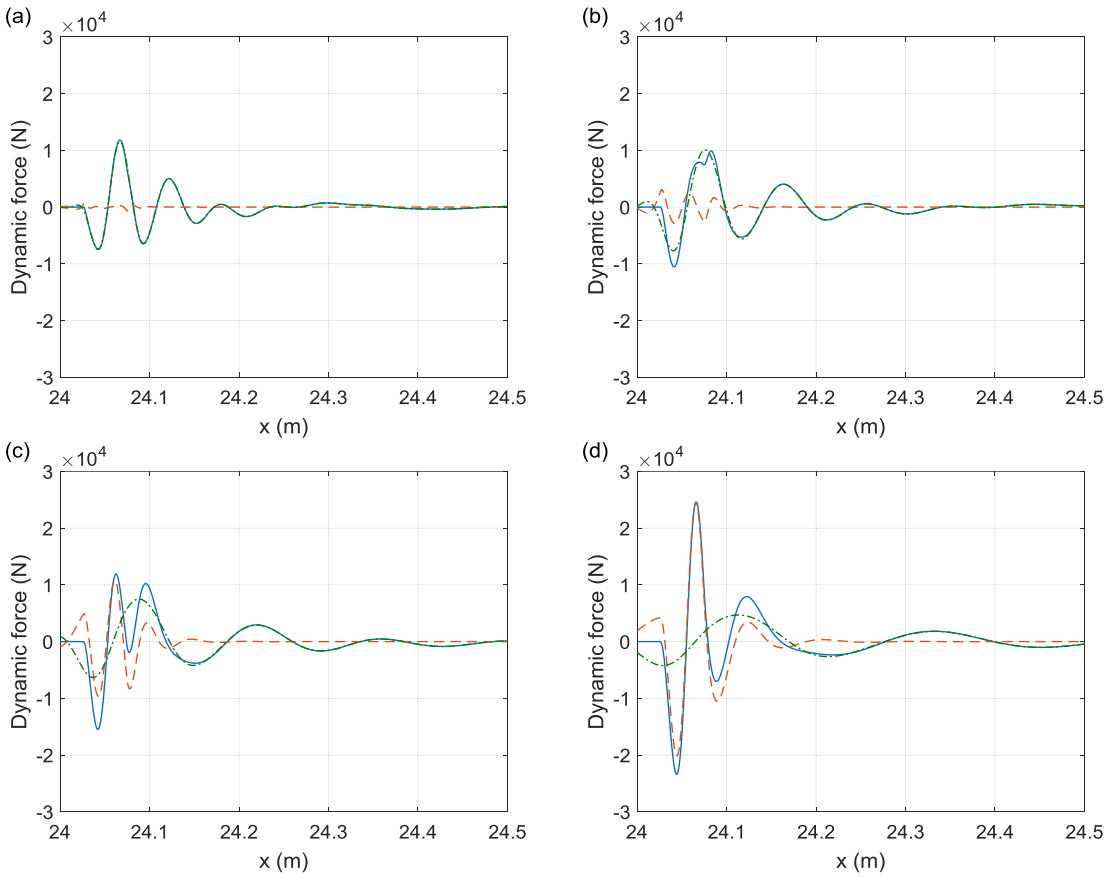

Fig. 27. Contact force when the vehicle moves over the defect shown in Fig. 24; total dynamic force (in blue), the high-frequency component of the dynamic force (in red) and the low-frequency component of the dynamic force (in green), at speeds of: (a) 50, (b) 80, (c) 120 and (d) 200 km/h. (For interpretation of the references to colour in this figure legend, the reader is referred to the web version of this article.)

increases as ride speed increases. At 80 km/h, it may be observed that the high-frequency component now has sufficient amplitude to modify the total force. At this speed, it may be observed that the total force shows a separation of peaks, thereby reducing the maximum contact force, as already explained for defects with a dip. The force is reduced because the high-frequency component and the low-frequency component are in anti-phase; therefore, when they are superimposed, they subtract from each other, and the split emerges in the peak of the total force.

At 120 km/h, the high-frequency component of the force has the same order of magnitude as the low-frequency component.

At this speed, it may now clearly be observed that it is the high-frequency component which generates the first peak of the contact force. This peak remains in almost the same position when the speed changes. This is because it is associated with the weld itself. The low-frequency component generates the second peak of the total force, which displaces in the spatial domain in the direction of travel, when the speed increases. Beyond this speed, the influence of the low-frequency component on the maximum peak becomes negligible in comparison to the influence of the high-frequency component. As the maximum peak of this high-frequency component increases with the speed, the maximum peak of the total force also increases with speed. However, the two peaks of the contact force are maintained, as may be observed, at 200 km/h. Depending on the discrepancy between the high-frequency and low-frequency components, one of the peaks of the total contact force will be the greater in absolute terms.

Fig. 28 shows the total dynamic forces and their high-frequency and low-frequency components for different speeds, when the wheel is moving over the track with a defect such as that shown in Fig. 24, but inverted, i.e. forming a protrusion. In this case, it may be observed that the shape of the maximum force/speed curve is practically linear, as it has no dips, and the contact force does not cease to increase at any speed. Fig. 28 shows that, for all speeds, the high-frequency and low-frequency components of the dynamic force combine as they are superimposed in positions at which the maximum peak of the force is located, and therefore the maximum contact force never diminishes.

Therefore, the separation of peaks of the force and their reduction in the case of welds with dips relates to the anti-phase of the high-frequency components (relating to the defect) and low-frequency components (relating to the wheelset-track

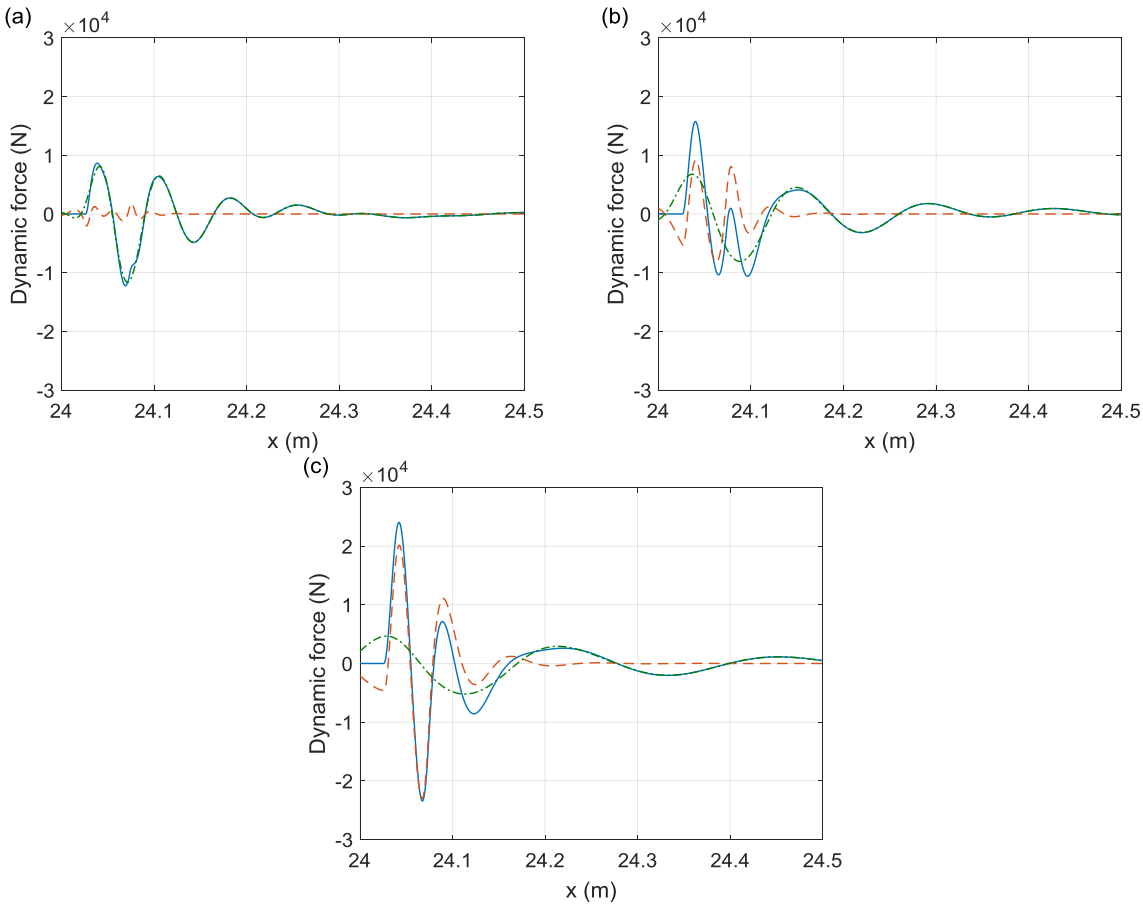

Fig. 28. Contact force when the vehicle moves over the inverted form of the defect shown in Fig. 24; the total dynamic force (in blue), the high-frequency component of the dynamic force (in red) and the low-frequency component of the dynamic force (in green), at speeds of: (a) 65 km/h, (b) 120 km/h and (c) 200 km/h. (For interpretation of the references to colour in this figure legend, the reader is referred to the web version of this article.)

system). On the other hand, in the case of welds with a negligible dip or no dip at all, there is no anti-phase between them at the point of maximum contact force, and thus the maximum value does not diminish when the speed increases, as observed in previous sections of the paper.

7. Discussion

This study analyses the maximum forces arising in the wheel-rail contact when a train moves over rail welds at different speeds. High values of these forces can induce rolling contact fatigue, causing cracks to initiate in weld defects. Specifically, this study focuses on the influence on contact forces of running speed and the position and geometry of the weld defect.

This study uses a track model in the spatial domain, which is described in Ref. [23], and obtained from the receptances calculated by an extremely accurate frequency-domain model based on the Periodic Structure Theory and the Finite Strip Method [32]. The spatial-domain model is obtained from the transformation between the domains of frequency and space using a Rational Fraction Polynomials method, which is modified with multiobjective genetic algorithms in order to improve the fitting of track receptance and to assist integration during simulations. This produces an accurate model with very short calculation times, a vital requirement for the study due to the large number of situations that had to be simulated (over 5000).

In general, it was observed that the parametric excitation of the track significantly influences the maximum forces during the displacements over welds, because the wheel moves over different positions on the track span. In most cases, when the defects of the weld were smoother, the track parametric excitation had a greater effect than the weld on the maximum forces at the contact.

In other types of defects, such as rail dipped joints, not only the maximum force but also the forces P1 and P2 increase linearly with running speed [11,13,24]; however, this is not always the case for weld defects. This study found that in the case of weld defects with a dip, the maximum force-speed curve rises to a relative maximum, and subsequently remains approximately constant or even diminishes within a generally wide range of speeds. Finally, the curve regains its rising trend.

It has been observed that the maximum force increases to a relative maximum and then diminishes in amplitude, because beyond the speed corresponding to this maximum, the maximum peak of the contact force in the spatial domain is divided into two. This forms a new force peak, thereby reducing the amplitude of the first peak. Thus, the maximum contact force is reduced.

It was shown that the formation of a new peak of the contact force was primarily due to the dynamics of the rail. In the spatial domain, it was ascertained that as the rail vibrates after the first peak in the contact force, it compresses against the wheel, generating a second peak in the force. Analysis of the high-frequency and low-frequency components of the force showed that the maximum force diminishes because the high-frequency portion (associated with the defect) and the low-frequency portion (associated with the wheelset-track system) are added or subtracted at each of the speeds. Until the force reaches its relative maximum, the high-frequency and low-frequency components combine. After the maximum value is reached, they begin to subtract, and therefore the maximum value of the contact force diminishes. Subsequently, at greater speeds, the two components of the force combine again, enabling the maximum force/speed curve to regain its ascending trend with respect to speed.

By establishing these maximum force/speed curves for several positions of the weld on the span, the 3D plot of the maximum force-speed-position of the weld is obtained. It was observed that when the welds have a dip, the shape of the 3D surface has a hollow (i.e. the combinations of speeds and positions of the weld defect on the track span for which the maximum force diminishes as speed increases).

On the other hand, for weld defects containing a protrusion without a dip or with a negligible dip, the increase in contact force with speed is much more linear. It was found that in these cases, the high-frequency and low-frequency components of the contact force combine at the maximum peak for all speeds, which means that the peak does not diminish.

In terms of the frequency composition of the contact forces, the force contains the same frequency components as that of the defect. The frequency components of the irregularity containing the most energy in the contact forces are those that coincide with the natural frequencies of the wheelset-track system. Therefore, the frequency components of the force with a greater amount of energy vary with the speed, as they are also associated with the wavelengths of the weld.

For a certain type of track and for each type of welding defect, this study shows the positions of the rail weld along the span between two sleepers at which the maximum contact forces would be the most severe when a train passes over the weld.

The limitation of the approach shown in this paper is that it does not allow drawing a single law that a priori serves for all welds regardless of their geometry. It remains open to a statistical study for each specific rail network, depending on how the geometry of its welds has turned out after welding and grinding. The state of the art study has shown that several papers [1–3,5] study the welding defects from a statistical point of view. The present paper provides the novelty of demonstrating the influence of the welding defect position with respect to the sleepers, and of distinguishing between two types of welding geometries. This is important, because it may help in the advancement of other statistical studies.

8. Conclusions

The main conclusions of this article are summarised as follows:

- A precise and very fast model has been presented for the study of contact forces when wheels pass over rail welds.
- For welding defects that have a dip as the fundamental characteristic in their geometry, the relationship between the maximum contact force and the running speed over welds is not linear (not even monotonically increasing).
  - This is due to the splitting of the maximum peak of the force into two, which results in a decrease in the maximum force. This splitting is caused by the high frequency component of the force (associated with the track vibration due to the welding defect). When the force has the maximum value, this high frequency component is in phase opposition to the low frequency component (associated with the system vehicle-track) for a range of velocities, thus decreasing the maximum value of the total force.
- In the case of welds whose fundamental characteristic is the presence of a protrusion without a dip or with a negligible dip, the relation between the maximum force and velocity is almost linear. This is because, in this case, the high and low frequency components are in phase when the total force attains the maximum value.
- The position of the weld along the span of the track has a great influence on the maximum values of the maximum contact force, especially in the welds that have dips. However, it is not possible to obtain the worst position for all weld defects and train speed ranges, as such position would depend on the weld geometry, the type of track and its dynamic parameters, as well as the axle-load and wheelset mass and dimensions, which also have an important influence on the parametric excitation and therefore on the wheel-rail contact forces.
- Comparing the results obtained, it can be concluded that, in general, if in the future this could be assured after the welding and grinding process, it would be preferable that the final welding geometry had dips instead of having protrusions (for equal amplitudes and main wavelengths), as this would lead to lower wheel-rail contact forces in a wider range of train speeds.

Acknowledgements

This work was partly financed by the European Horizon 2020 Joint Technology Initiative Shift2Rail through contract No 730841. The authors also wish to thank the Spanish Research Ministry MICINN/Economy and Competitiveness Ministry MINECO for their funding through contract TRA2014-59599-R, including funding by the FEDER-ERDF European Regional Development Fund, and also the Basque Government for financial assistance through IT919-16. The financial assistance received from UPV/EHU through the training and research unit UFI11/29 is likewise gratefully acknowledged.

References

[1] M.J.M.M. Steenbergen, C. Esveld, Rail weld geometry and assessment concepts, J. Rail Rapid Transit 220 (2006) 257–271, https://doi.org/10.1243/09544097JRRT38.
[2] M.J.M.M. Steenbergen, Quantification of dynamic wheel–rail contact forces at short rail irregularities and application to measured rail welds, J. Sound Vib. 312 (2008) 606–629, https://doi.org/10.1016/j.jsv.2007.11.004.
[3] M.J.M.M. Steenbergen, Wheel-rail Interaction at Short-wave Irregularities, Ph.D. Thesis, Delft University of Technology, 2008.
[4] Z. Wen, G. Xiao, X. Xiao, X. Jin, M. Zhu, Dynamic vehicle–track interaction and plastic deformation of rail at rail welds, Eng. Fail. Anal. 16 (2009) 1221–1237, https://doi.org/10.1016/j.engfailanal.2008.08.001.
[5] I. Grossoni, P. Shackleton, Y. Bezin, J. Jaiswal, Longitudinal rail weld geometry control and assessment criteria, Eng. Fail. Anal. 80 (2017) 352–367, https://doi.org/10.1016/j.engfailanal.2017.07.008.
[6] L. Baeza, P. Vila, G. Xie, S.D. Iwnicki, Prediction of rail corrugation using a rotating flexible wheelset coupled with a flexible track model and a non-Hertzian/non-steady contact model, J. Sound Vib. 330 (2011) 4493–4507, https://doi.org/10.1016/j.jsv.2011.03.032.
[7] P. Vila, L. Baeza, J. Martínez-Casas, J. Carballeira, Rail corrugation growth accounting for the flexibility and rotation of the wheel set and the non-Hertzian and non-steady-state effects at contact patch, Veh. Syst. Dyn. 52 (2014) 92–108, https://doi.org/10.1080/00423114.2014.881513.
[8] P.A. Meehan, R.D. Batten, P.A. Bellette, The effect of non-uniform train speed distribution on rail corrugation growth in curves/corners, Wear 366–367 (2016) 27–37, https://doi.org/10.1016/j.wear.2016.05.009.
[9] H. Zhang, W. Liu, W. Liu, Z. Wu, Study on the cause and treatment of rail corrugation for Beijing metro, Wear 317 (2014) 120–128, https://doi.org/10.1016/j.wear.2014.05.011.
[10] N. Correa, E.G. Vadillo, J. Santamaria, J. Herreros, A versatile method in the space domain to study short-wave rail undulatory wear caused by rail surface defects, Wear 352–353 (2016) 196–208, https://doi.org/10.1016/j.wear.2016.02.012.
[11] Y.Q. Sun, C. Cole, M. Spiryagin, Study on track dynamic forces due to rail short-wavelength dip defects using rail vehicle-track dynamics simulations, J. Mech. Sci. Technol. 27 (2013) 629–640, https://doi.org/10.1007/s12206-013-0117-8.
[12] I. Grossoni, S. Iwnicki, Y. Bezin, C. Gong, Dynamics of a vehicle–track coupling system at a rail joint, Proc. Inst. Mech. Eng. Part F J. Rail Rapid Transit 229 (2015) 364–374, https://doi.org/10.1177/0954409714552698.
[13] N.K. Mandal, M. Dhanasekar, Y.Q. Sun, Impact forces at dipped rail joints, Proc. Inst. Mech. Eng. Part F J. Rail Rapid Transit 230 (2016) 271–282, https://doi.org/10.1177/0954409714537816.
[14] B. Liang, S.D. Iwnicki, Y. Zhao, D. Crosbee, Railway wheel-flat and rail surface defect modelling and analysis by time–frequency techniques, Veh. Syst. Dyn. 51 (2013) 1403–1421, https://doi.org/10.1080/00423114.2013.804192.
[15] J. Pombo, J. Ambrósio, M. Pereira, R. Verardi, C. Ariaudo, N. Kuka, Influence of track conditions and wheel wear state on the loads imposed on the infrastructure by railway vehicles, Comput. Struct. 89 (2011) 1882–1894, https://doi.org/10.1016/j.compstruc.2011.05.009.
[16] R. Licciardello, G. Malavasi, A. Tieri, P. Vitali, Reference values for railway sidings track geometry, Transp. Res. Procedia 14 (2016) 1996–2005, https://doi.org/10.1016/j.trpro.2016.05.167.
[17] A. Ekberg, B. Åkesson, E. Kabo, Wheel/rail rolling contact fatigue – probe, predict, prevent, Wear 314 (2014) 2–12, https://doi.org/10.1016/j.wear.2013.12.004.
[18] J.I. Egana, J. Vinolas, M. Seco, Investigation of the influence of rail pad stiffness on rail corrugation on a transit system, Wear 261 (2006) 216–224, https://doi.org/10.1016/j.wear.2005.10.004.
[19] S.L. Grassie, Rail corrugation: characteristics, causes, and treatments, Proc. Inst. Mech. Eng. Part F J. Rail Rapid Transit 223 (2009) 581–596, https://doi.org/10.1243/09544097JRRT264.
[20] M.H. Richardson, D.L. Formenti, Parameter estimation from frequency response measurements using rational fraction polynomials, in: 1st International Modal Analysis Conference, Orlando, FL, 1982.
[21] T.X. Wu, D.J. Thompson, On the parametric excitation of the wheel/track system, J. Sound Vib. 278 (2004) 725–747, https://doi.org/10.1016/j.jsv.2003.10.047.
[22] T.X. Wu, Parametric excitation of wheel/track system and its effects on rail corrugation, Wear 265 (2008) 1176–1182, https://doi.org/10.1016/j.wear.2008.01.025.
[23] N. Correa, E.G. Vadillo, J. Santamaria, J. Gómez, A rational fraction polynomials model to study vertical dynamic wheel–rail interaction, J. Sound Vib. 331 (2012) 1844–1858, https://doi.org/10.1016/j.jsv.2011.12.012.
[24] H. Jenkins, J. Stephenson, G. Clayton, G. Morland, D. Lyon, The effect of track and vehicle parameters on wheel/rail vertical dynamic forces, Railw. Eng. J. 3 (1974).
[25] N. Correa, E.G. Vadillo, J. Santamaria, J. Gómez, On the study of train–track dynamic interactions caused by rail welds on discrete supported rails, Wear 314 (2014) 291–298, https://doi.org/10.1016/j.wear.2013.11.044.
[26] J.C.O. Nielsen, A. Igeland, Vertical dynamic interaction between train and track influence of wheel and track imperfections, J. Sound Vib. 187 (1995) 825–839, https://doi.org/10.1006/jsvi.1995.0566.
[27] T.X. Wu, D.J. Thompson, A hybrid model for the noise generation due to railway wheel flats, J. Sound Vib. 251 (2002) 115–139, https://doi.org/10.1006/jsvi.2001.3980.
[28] A. Johansson, J.C.O. Nielsen, Out-of-round railway wheels—wheel-rail contact forces and track response derived from field tests and numerical simulations, Proc. Inst. Mech. Eng. Part F J. Rail Rapid Transit 217 (2003) 135–146, https://doi.org/10.1243/095440903765762878.
[29] A Pieringer, W Kropp, A fast-time-domain model for wheel/rail interaction demonstrated for the case of impact forces caused by wheel flats, Proceedings of Acoustics '08, Paris, France, June 29-July 4 2008.
[30] A. Pieringer, W. Kropp, J.C.O. Nielsen, The influence of contact modelling on simulated wheel/rail interaction due to wheel flats, Wear 314 (2014) 273–281, https://doi.org/10.1016/j.wear.2013.12.005.
[31] T.X. Wu, D.J. Thompson, On the impact noise generation due to a wheel passing over rail joints, J. Sound Vib. 267 (2003) 485–496, https://doi.org/10.1016/S0022-460X(03)00709-0.
[32] J. Gómez, E.G. Vadillo, J. Santamaría, A comprehensive track model for the improvement of corrugation models, J. Sound Vib. 293 (2006) 522–534, https://doi.org/10.1016/j.jsv.2005.08.064.
[33] X. Sheng, X. Xiao, S. Zhang, The time domain moving Green function of a railway track and its application to wheel–rail interactions, J. Sound Vib. 377 (2016) 133–154.
[34] T. Mazilu, M. Dumitriu, C. Tudorache, M. Sebeşan, Using the Green's functions method to study wheelset/ballasted track vertical interaction, Math. Comput. Model. 54 (2011) 261–279.